

# DenseShift : Towards Accurate and Transferable Low-Bit Shift Network

Xinlin Li <sup>1</sup>, Bang Liu <sup>2</sup>, Rui Heng Yang <sup>1</sup>, Vanessa Courville <sup>1</sup>, Chao Xing <sup>1</sup>, Vahid Partovi Nia <sup>1</sup>

<sup>1</sup> Noah’s Ark Lab, Huawei Technologies.

<sup>2</sup>Department of Computer Science and Operations Research (DIRO), University of Montreal.

## Abstract

Deploying deep neural networks on low-resource edge devices is challenging due to their ever-increasing resource requirements. Recent investigations propose multiplication-free neural networks to reduce computation and memory consumption. Shift neural network is one of the most effective tools towards these reductions. However, existing low-bit shift networks are not as accurate as their full precision counterparts and cannot efficiently transfer to a wide range of tasks due to their inherent design flaws. We propose *DenseShift* network that exploits the following novel designs. First, we demonstrate that the zero-weight values in low-bit shift networks are neither useful to the model capacity nor simplify the model inference. Therefore, we propose to use a zero-free shifting mechanism to simplify inference while increasing the model capacity. Second, we design a new metric to measure the weight freezing issue in training low-bit shift networks, and propose a sign-scale decomposition to improve the training efficiency. Third, we propose the low-variance random initialization strategy to improve the model’s performance in transfer learning scenarios. We run extensive experiments on various computer vision and speech tasks. The experimental results show that DenseShift network significantly outperforms existing low-bit multiplication-free networks and can achieve competitive performance to the full-precision counterpart. It also exhibits strong transfer learning performance with no drop in accuracy.

## Introduction

Deep neural networks have achieved superior performance in a variety of tasks, including image classification (He et al. 2016b), object detection (Liu et al. 2016), image segmentation (Chen et al. 2017), and so on. However, this performance comes at the cost of increased model size, which leads to a higher computational complexity due to the increased amount of floating-point multiplication in training and inference time, yielding a higher memory footprint and increasing energy consumption. To reduce computational complexity, researchers are exploring multiplication-free neural networks.

Existing works on multiplication-free neural networks include binary (Courbariaux, Bengio, and David 2015), and ternary quantization (Li, Zhang, and Liu 2016). They respectively constrain their weights in the range of  $\{\pm 1\}$  and  $\{0\} \cup \{\pm 1\}$ , so that the less expensive sign flip operator

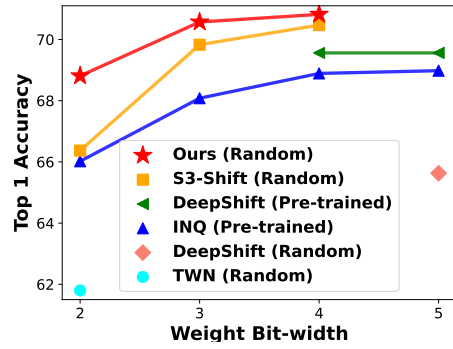


Figure 1: Benchmark low-bit DenseShift networks over SOTA low-bit Shift networks on ImageNet using the ResNet-18 model architecture.

can implement the multiplication operations. Such low-bit quantization techniques can help deploy deep learning models on resource-constrained edge devices. Moreover, Wang et al. (2021) trades the multiplication operation with the addition operation, and Elhoushi et al. (2019); Li et al. (2021); Przewlocka-Rus et al. (2022) use the bit-shift operator to build power-of-two (PoT) quantized networks, also named shift networks. For shift networks built on a ternary base, their weight space includes  $\{0\} \cup \{\pm 2^p\}$ . In such a weight space, the multiplication operations are equivalent to bit-wise shift operations, which are highly efficient in terms of hardware implementation. As a demonstration, Przewlocka-Rus et al. (2022) shows that under 4-bit weight and 8-bit activation, the shift-based MAC unit designed for shift networks outperformed its counterpart for traditional uniform quantization by 2.4x energy saving and 20% chip area saving using Samsung 5nm.

Specifically, a recent study (Li et al. 2021) proposes a weight reparameterization scheme  $S^3$  for shift network training, which significantly improves the accuracy of the ImageNet classification task under sub-4bits condition. It shows that the poor performance of previous shift networks are caused by the design of the ternary quantizer, which prevents the discrete weight value across zero, leading to their weight sign cannot easily change during training. This phenomenon is called weight freezing. While  $S^3$  outperforms

previous shift networks, it has the following shortcomings: i)  $S^3$  exploits a low weight bit-width, which causes performance drop under low-bit conditions compared to full-precision networks; ii)  $S^3$  fails to explain the weight freezing problem for non-ternary quantizers, and the handling of zero weights increases the computational complexity during inference; iii)  $S^3$  is only benchmarked on the image classification task and suffers significant performance degradation under 2-bit conditions. The transfer learning tasks are unexplored.

In this work, we investigate and analyze the design flaws of existing low-bit shift networks and propose a new *DenseShift* network that exploits several novel designs based on our analysis. Our contributions help improve the model capacity, training efficiency, and model transferability. We shall introduce as follows.

First, our analysis demonstrates that the zero weights in low-bit shift networks lead to downgraded model capacity under limited bit widths and increase the complexity of model inference. To solve this issue, we remove zero value in the weight space and propose to use zero-free shifting under low-bit conditions. Compared to existing low-bit shift networks, such a design has better inference efficiency and model representation capacity, which is critical for a good performance in low-bit conditions.

Second, to thoroughly investigate the weight freezing issue brought by Li et al. (2021), we design a new metric for measuring the extent of weight freezing. It averages the weights' filter-wise cosine similarities throughout the training epochs, and a high similarity indicates the existence of weight freezing. Inspired by Li et al. (2021), we design a sign-scale decomposition to decompose the discrete weights of *DenseShift* networks into a binary sign term and a power-of-two scale term. By recursively re-parameterizing the exponent of the scale term as a combination of binary variables, we can address the weight freezing issue and improve the training efficiency.

Third, while prior research works suffer from severe performance degradation when transferred to a new task, we propose a low-variance random initialization strategy to improve the model's performance in transfer learning scenarios. This is based on our observation and analysis that the weight values tend to gather towards the original point of the re-parameterization space during the initial stage of training, and a greater gradient signal is needed to push them to pass the threshold when the weights are randomly initialized with a large variance. By reducing the variance of weight initialization, the *DenseShift* network can be easily adapted to different tasks and achieve competitive performance.

We perform extensive experiments to compare our *DenseShift* network with various baselines on a range of tasks across different fields. The results show that our proposed *DenseShift* network outperforms the state-of-the-art shift network on the ImageNet classification task and achieves comparable performance as full-precision networks with higher inference computational efficiency. As summarized in Fig. 1, *DenseShift* network performs significant better in low bit settings, especially under 2-bit condition. Specifically, our 2-bit and 3-bit quantized ResNet-18 on the clas-

sification task achieve 68.90% and 70.57% Top-1 accuracy respectively. Furthermore, we show that low-bit *DenseShift* networks can achieve full-precision performance in transfer learning scenarios and different domains by experiments on several computer vision (CV) and speech tasks, which to the best of our knowledge is for the first time in shift networks for transfer learning tasks.

## Related Works

Different approaches have been suggested to replace the expensive multiplication operation to mitigate the computational complexity of neural networks. Low-bit neural networks with binary weights (Courbariaux, Bengio, and David 2015; Rastegari et al. 2016) or ternary weights (Li, Zhang, and Liu 2016) are examples of multiplication free networks. While computationally inexpensive, their major flaw lies in the accuracy gap compared to their full-precision counterparts, as they suffer from under-fitting on large datasets. There are also works that utilize computationally cheaper operations, such as addition operations (Chen et al. 2020; Wang et al. 2021; Xu et al. 2020), square operations (Prazeres et al. 2021), or bit-shift operations (Zhou et al. 2017; Gudovskiy and Rigazio 2017; Elhoushi et al. 2019; Miyashita, Lee, and Murmann 2016). Compared to using binary or ternary weights, these methods achieve a low accuracy drop on large datasets but require higher weight representation bit-width as a trade-off. Some other works try to improve the performance of multiplication-free neural networks by using both addition and bit-shift operations (You et al. 2020), a sum of binary bases (Lin, Zhao, and Pan 2017; Zhang et al. 2018), or sum of shift kernels (Li, Dong, and Wang 2019), however, they remain computational costly as more operations are used per kernel.

Li et al. (2021) proposes a weight reparameterization technique  $S^3$  for training low-bit shift networks. It points out the design flaw of the weight quantizer for low-bit shift networks and proposes to decompose a discrete parameter in a sign-sparse-shift 3-fold manner to improve training efficiency. Compared to Li et al. (2021), in the *DenseShift* network, the zero-free weight space further improves the model representation capacity and inference efficiency. Besides, along with a new metric for measuring weight freezing, the sign-scale decomposition of *DenseShift* better addresses the issue and improves the training efficiency. Last but not least, the low-variance random initialization strategy equips low-bit shift networks with strong transferability, which is what  $S^3$  lacks.

## *DenseShift* Network

In this section, we describe our observations and analysis of the design of existing low-bit shift networks and introduce our proposed *DenseShift* in terms of weight space design, training mechanism, and weight initialization strategy.

### *DenseShift* with Zero-Free Shifting

We begin with the analysis of the weight space of shift networks. A weight space with  $n$ -bit can encode up to  $2^n$  discrete weight values. Since the zero value has no correspond-

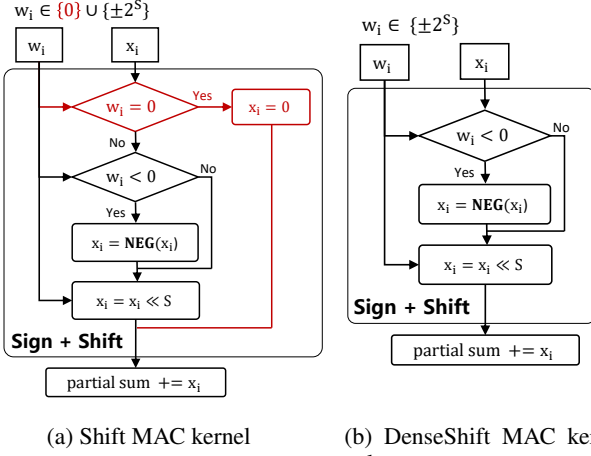


Figure 2: Compare the Multiply-Accumulate (MAC) operations in Shift and DenseShift. The DenseShift MAC is more efficient as its  $w_i$  excludes zero.

ing negative value, the encoding space utilization rate is reduced to  $\frac{2^n-1}{2^n}$  in previous shift networks. Under the high-bit condition, this waste ratio is insignificant and is often ignored. However, under low-bit, especially when  $n \leq 4$ , an extra encoding space plays a crucial role. For example, the encoding rate is only 75% with zero-weight value in a 2-bit weight space.

DenseShift fully utilizes all available encoding space by dropping the zero value in the weight space, significantly outperforming previous shift networks under limited model capacity, especially under low-bit weight conditions. With a zero-free weight space design, DenseShift is simpler to compute when compared to shift networks as there is no need to include the hardware support for zero-weights. Figure 2 compares the Multiply-Accumulate (MAC) operation between DenseShift and shift networks. We can observe from Fig. 2a that the fixed-point dot product operation in existing shift networks receives two fixed-point input vectors: the activations  $x_i$ , and the weights  $w_i$  that are encoded by its shift value  $S$ . The shift operation is performed by first sign-flipping  $x_i$ , shifting the result by its corresponding shift value  $S_i$ , and accumulating over all data points. However, special handling is required when  $w_i = 0$  to bypass these operations and simply pass a value of  $x_i = 0$  to the accumulator instead. Since DenseShift networks guarantee that  $w_i$  will never be zero, this conditional branch is no longer required, as shown in Fig. 2b. Therefore, the inference computation in DenseShift networks is more straightforward than in existing shift networks.

As a demonstration, we compare DenseShift networks to existing shift networks through a vectorized software implementation to show its advantage in computational efficiency.

Specifically, we implement *DenseShift* kernel and *Shift* kernel for dot-product computation on ARM A57 CPU using NEON SIMD architecture and count the average time consumption. Due to the limitations of ARM neon intrinsic data types, we consider 8-bit weights as a proof-of-concept. We run experiments for 4096 data points. The results aver-

aged over 1000 runs show that the latency for the Shift network and our DenseShift network are  $2.65\mu s$  and  $1.79\mu s$ , respectively. In other words, the *DenseShift* kernel obtains 1.48X speed-up compared to a *Shift* kernel implementation.

Aside from experimental demonstration, we also theoretically show that removing zeros from the weight space doesn't affect the representation power of DenseShift models. The theorems are shown as follows, and the detailed proofs of them are described in the Appendix:

**Theorem 1.** *Every shift network has a DenseShift representation.*

Theorem 1 confirms that there is a DenseShift network that can reach to the same accuracy of any shift network if properly trained. However, practitioners are usually interested in finding a DenseShift that has a similar capacity to a full-precision network rather than a shift network, which motivates us to build Theorem 2.

**Theorem 2.** *A DenseShift network with a L-Lipschitz activation function is a universal approximator on a compact set  $K$  for any measurable continuous function  $f \in C(K)$  with respect to the measure  $\mu$ , if the dense shift network with weight and feature  $\mathbf{w}', \mathbf{x}'$  remains close to the regular network with weight and features  $\mathbf{w}, \mathbf{x}$  in the following sense*

$$\int_K \left( \sum_{j=1}^J \sum_{k=1}^{d_j} (\mathbf{w}_k \mathbf{x}_k^j - \mathbf{w}'_k \mathbf{x}'_k^j) \right)^2 d\mu < \frac{\epsilon}{4L}$$

where  $\frac{\epsilon}{4}$  is the approximation quality of the full-precision neural network.

Theorem 2 assures a DenseShift network behaves like the common full-precision networks if the inner products between features and weights of a DenseShift network remain close to the full precision. Although the zero-free shifting design makes the model incompatible with the non-structural pruning technique (Han, Mao, and Dally 2015), we argue that it is impractical to prune a low-bit DenseShift network with the number of bits  $n \leq 4$ . That is because the sparse matrix format is inefficient in the low-bit situation as it stores non-zero values and indexes them in pairs. For instance, a typical CNN kernel size is  $3 \times 3 \times 256 \times 256 > 2^{16}$ . Each sub-4bits weight value may require a uint32 index, making memory usage inefficient.

## Weight Freezing in Low-Bit Network Training

In this part, we analyze existing training methods for shift networks, particularly the quantizer-based methods and discrete weight reparameterization methods. We will show that the inherent design flaw of existing quantizer-based methods causes the downgraded performance of shift networks compared to their full-precision counterparts.

We begin our analysis with the quantizer-based training methods. Przewlocka-Rus et al. (2022) designs a symmetric quantizer to discretize the continuous weights, but this training method may not converge when training from scratch, as pointed out by the authors. Elhoushi et al. (2019) represents a discrete weight parameter as the product of a ternary

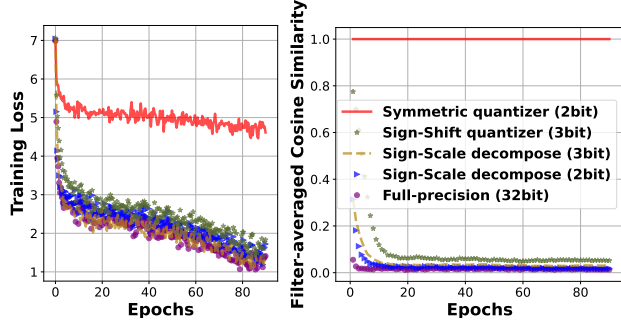


Figure 3: Compare different training methods for the DenseShift network with the full-precision baseline. The symmetric quantizer is adapted from Przewlocka-Rus et al. (2022), and the sign-shift quantizer is adapted from Elhoushi et al. (2019). The sign-scale decomposition is our proposed training method. Left: All training methods can reduce training loss. Right: The filter-averaged cosine similarities between the initial and current epoch of the first quantized convolution layer in a ResNet-18 model during training on the ImageNet classification task. This figure shows that the quantizer-trained low-bit filters correlate to its initialization on average and imply the weight freezing issue, while the full-precision baseline and our method can almost reach zero averaged cosine similarity when the model converged.

weight base and a PoT scaling factor and utilizes two quantizers to learn them respectively, but suffers from severe performance drop when trained from scratch. Similar issues are observed when we adopt these two quantizer-based methods to DenseShift training. Therefore, we investigate why the training methods are ineffective and try to find a remedy.

Previously, Li et al. (2021) pointed out that when the ternary weights are trained with a quantizer, the weight cannot easily cross zero to switch their sign. However, it didn't explain the training difficulty of a non-ternary symmetric quantizer. Since DenseShift networks have no zero weight value, it further motivates us to develop a deeper understanding of this optimization difficulty. Our analysis shows that the issue is the *weight freezing* originated from the quantizer.

Weight freezing happens when a quantizer attempts to learn highly discrete weights from continuous weights: the weights tend to concentrate around the quantizer's threshold values, making it difficult to be pushed away by the gradient signals in back-propagation. In this scenario, the backward gradient signals cannot fully adjust these concentrated weight values, so the model fails to explore the space properly. We observe that such weight freezing issue occurs to low-bit quantizers except for the binary one.

To visualize the extent of weight freezing, we design a new metric which averages the weights' filter-wise cosine similarities between the initial and current epochs. Ideally, the metric value should be close to zero at the end of the training stage, meaning that the trained filters are expected to be irrelevant to their initialization. With this assumption, the model can train from a random initial state and converge to a good state. Figure 3 shows that the assumption holds for full-precision networks: the filter-averaged cosine similarity

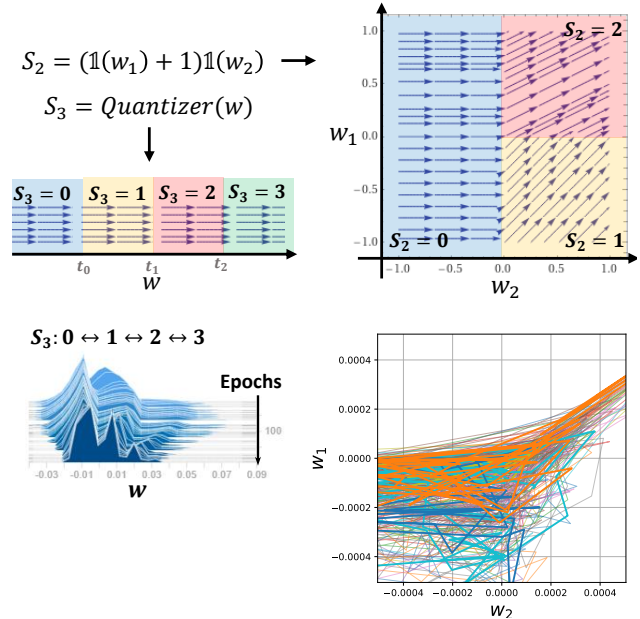


Figure 4: Top Left: The optimization space of the shifting parameter  $S_3$  defined by the sign-shift quantizer. The arrow direction represents the moving direction of the continuous weight  $w$  in the optimization space when the gradient update of the shifting parameter  $S_T$  is positive. Bottom Left: The actual continuous weight histogram variation of  $S_3$  defined by the 3-bit sign-shift quantizer during training. Top Right: The phase plane of the re-parameterization space of  $S_2$  defined by a recursive product of binary variables ( $\frac{\partial w_2}{\partial t} = \mathbb{1}(w_1) + 1$ ,  $\frac{\partial w_1}{\partial t} = \mathbb{1}(w_2)$ ). Bottom Right: Some sampled actual weight traces of  $S_2$  on the optimization space defined by a recursive product of binary variables during training.

maintains close to zero during the training process. However, when training a low-bit DenseShift network using the quantizer-based methods, the metric remains far from zero until the end of the training, which differs significantly from its full-precision counterpart.

## Sign-Scale Decomposition for Efficient Training

In this part, we propose an efficient training algorithm for DenseShift to solve the issue of weight freezing and achieve a performance comparable to its full-precision counterpart.

We propose to use sign-scale decomposition inspired by (Li et al. 2021), which design is to promote weight-sign switching during training. We found that this decomposition is an effective remedy for the weight freezing issue and propose to decompose the discrete weight of DenseShift networks into two parts: a binary base term  $w_{\text{sign}}$  and a PoT scale term which shifts the input activation for  $S$  bits:

$$w_{\text{shift}} = \underbrace{\{2\mathbb{1}(w_{\text{sign}}) - 1\}}_{\text{Sign}} \underbrace{2^{S_T}}_{\text{Scale}}, \quad (1)$$

where  $\mathbb{1}(\cdot)$  is the Heaviside function mapping all positive

values to one and the remaining to zero.

Next, we recursively re-parameterize the shifting parameter  $S$  as a combination of  $t$  binary variables to address the weight freezing problem:

$$S_0 = 0, S_t = \mathbb{1}(w_t)(S_{t-1} + 1). \quad (2)$$

In the following, we demonstrate the re-parameterization on positive  $S$  values using 3-bit case as an example, and the negative  $S$  values can be obtained by adding a constant bias term. Define a 3-bit DenseShift network with discrete weights  $w_{\text{shift}} \in \{\pm 1, \pm 2, \pm 4, \pm 8\}$ . This network can be re-parameterized as:

$$w_{\text{shift}} = \{2 \mathbb{1}(w_{\text{sign}}) - 1\} 2^{S_3}, \quad (3)$$

$$S_3 = \mathbb{1}(w_3) \{ \mathbb{1}(w_2) \{ \mathbb{1}(w_1) + 1 \} + 1 \}. \quad (4)$$

Note that all the weights  $\{w_{\text{sign}}, w_1, w_2, w_3\}$  are trained in full-precision. By representing the original shift parameter  $S_3$  with three full-precision parameters  $w_1, w_2$ , and  $w_3$ , we are projecting the optimization process from 1D space to higher-dimensional 3D space, making the shift parameter easier to vary between different scales and thus easier to learn. While such training requires  $(N + 1)$  floating point references, it is not as memory expensive as it appears, especially under 2/3-bit weight conditions. The memory is dominated by the activation with a large batch size during training.

To better explain why the weight re-parameterization approach addresses the weight freezing issue, in Fig. 4, we visualize the optimization spaces of the shifting parameter  $S$  defined i) by a quantizer (figure left part) and ii) by a recursive product of binary variables (figure right part). In the quantizer's optimization space, the continuous weights accumulate at the three discontinuities of the quantizer. This implies that the weights attracted by the discontinuities could not move freely on the optimization space. In contrast, the weights in the optimization space defined by the recursive product of binary variables are gathered at the origin of the optimization space during training, and the value of the shifting parameter  $S$  can vary easily according to the gradient update signal. The visualization shows our re-parameterization promotes the shifting parameters  $S$  to oscillate in an extensive range value during training instead of oscillating around the quantizer's threshold values. This design reduces the optimization space's rigidness, thus solving the weight freezing problem and allowing the model to converge to a better solution. Note that using more weight parameters to represent the shift parameter  $S$  almost doesn't affect the memory consumption, as the memory consumption is dominated by the activation calculations when training with a large batch size.

The local learning rate of individual parameter  $w_{\text{sign}}$  in the proposed training scheme is significantly larger than the global learning rate on the discrete weight  $w_{\text{shift}}$ . Furthermore, we analyze the backward gradient computation of our proposed decomposition. We estimate the backward gradient across the Heaviside function using a Straight-Through-Estimator (STE) (Bengio 2013). The gradient update towards  $w_{\text{sign}}$  is calculated as:

$$\frac{\partial \text{Loss}}{\partial w_{\text{sign}}} = \frac{\partial \text{Loss}}{\partial w_{\text{shift}}} 2^{S_T}, \quad (5)$$

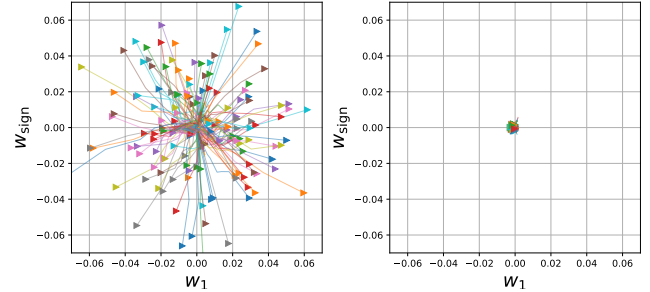


Figure 5: Re-parameterized weight trace visualization of a 2-bit DenseShift ResNet-18 trained on ImageNet dataset, the “triangle” indicates the initial point. Left panel: Kaiming initialization. Right panel: Low-variance initialization.

where  $2^{S_T} \in \{1, 2, \dots, 2^T\}$ . From Eq. 5 we observe that  $2^{S_T}$  plays a role of learning rate scale factor, and it has an extensive value range. Hence, it may significantly impact the gradient update scale. Based on our observation, we propose a local learning rate re-scaling strategy to address this issue. We replace Eq. 5 with Eq. 6 during backward propagation to re-scale local gradient updates:

$$\frac{\partial \text{Loss}}{\partial w_{\text{sign}}} = \frac{\partial \text{Loss}}{\partial w_{\text{shift}}} \sqrt{S_T + 1}. \quad (6)$$

### Low-Variance Random Initialization for Transfer Learning

We encountered difficulties when applying the above method in the transfer learning scenario. Most transfer learning tasks follow the following training paradigm: i) Pre-train a backbone model on a large dataset; ii) Remove and add new layers to the backbone model and randomly initialize the new layer; iii) Finetune the new model on a downstream task. During our experiments, we noticed that when we finetune a pre-trained DenseShift backbone with randomly-initialized DenseShift layers in an end-to-end manner, the model suffers from severe performance degradation or loss divergence. Such performance degradation also exists for existing shift networks.

We analyzed the difference between the pre-trained weights and the randomly-initialized weights in the DenseShift model and noticed that the variance of the former is much lower than that of the latter. To better understand this phenomenon, we trained a 2-bit DenseShift network and noticed that when using the default Kaiming initialization (He et al. 2015), the weight values tend to gather towards the origin point of the re-parameterization space during the first few training epochs, as shown in figure 5. This indicates that the initialized weight values are too far from the centre, an unwanted behaviour. More precisely, the weight values are far from the thresholds, meaning a greater initial gradient signal is needed to push them to pass the thresholds. In the transfer learning scenario, the backbone weight values are easier to change than the new Kaiming initialized layers. In fact, we argue that it is precisely this behavior that damages

| Kernel            | Methods      | W Bits   | Init. | Top-1 (%)    |
|-------------------|--------------|----------|-------|--------------|
| Multi.            | FP32         | 32       | R     | 69.6         |
|                   | TTQ          | 2        | PT    | 66.6         |
| Sum of Sign Flips | Lq-Net       | 2        | R     | 68.0         |
|                   | Lq-Net       | 3        | R     | 69.3         |
|                   | Lq-Net       | 4        | R     | 70.0         |
| Sign Flip         | BWN          | 1        | R     | 60.8         |
|                   | HWGQ         | 1        | R     | 61.3         |
|                   | BWHN         | 1        | R     | 64.3         |
|                   | IR-net       | 1        | R     | 66.5         |
|                   | TWN          | 2        | R     | 61.8         |
|                   | LR-net       | 2        | R     | 63.5         |
|                   | SQ-TWN       | 2        | R     | 63.8         |
|                   | INQ          | 2        | PT    | 66.02        |
|                   | $S^3$ -Shift | 2        | R     | 66.37        |
|                   | <b>Ours</b>  | <b>2</b> | LVR   | <b>68.90</b> |
| Shift + Sign Flip | INQ          | 3        | PT    | 68.08        |
|                   | INQ          | 4        | PT    | 68.89        |
|                   | INQ          | 5        | PT    | 68.98        |
|                   | DeepShift    | 5        | R     | 65.63        |
|                   | DeepShift    | 4        | PT    | 69.56        |
|                   | DeepShift    | 5        | PT    | 69.56        |
|                   | $S^3$ -Shift | 3        | R     | 69.82        |
|                   | <b>Ours</b>  | <b>3</b> | LVR   | <b>70.57</b> |
|                   | $S^3$ -Shift | 4        | R     | 70.47        |
|                   | <b>Ours</b>  | <b>4</b> | LVR   | <b>70.82</b> |

Table 1: Comparison of SOTA methods using DenseShift ResNet-18 architecture trained on ImageNet. Initialization defined as: R is Kaiming Normal Random, PT is Pre-Trained, LVR is Low-Variance Random.

the pre-trained backbone during transfer learning.

To easily transfer a DenseShift network to other tasks, we suggest randomly initializing all re-parameterized variables with a small standard deviation. We name it low-variance random initialization. Specifically, we chose a standard deviation of  $10^{-3}$  for all the experiments in this paper. The experiments demonstrate that our low-variance random initialization strategy is required for achieving competitive performance on transfer learning tasks such as object detection and semantic segmentation.

## Experiments

### ImageNet Classification

**Model and Dataset:** We benchmark our proposed method with different bit-widths. To verify the effectiveness and robustness, we apply DenseShift to ResNet-18/50/101 architectures and evaluate on ILSVRC2012 dataset (Deng et al. 2009) with data augmentation and pre-processing strategy proposed in (He et al. 2016a). Following (Rastegari et al. 2016; Liu et al. 2018; Zhang et al. 2018), all but the first convolution layers are quantized.

**Experiment Results:** Results are shown in table 1 and 2. We compare our proposed method with SOTA low-bit multiplication-free networks using binary weights (Rastegari et al. 2016; Cai et al. 2017; Hu, Wang, and Cheng

| ResNet-50         |              |          |       |              |
|-------------------|--------------|----------|-------|--------------|
| Kernel            | Methods      | W Bits   | Init. | Top-1 (%)    |
| Multi.            | FP32         | 32       | R     | 76.00        |
|                   | Lq-Nets      | 2        | R     | 75.10        |
| Sum of Sign Flips | Lq-Nets      | 4        | R     | 76.40        |
|                   | INQ          | 5        | PT    | 74.81        |
|                   | DeepShift    | 6        | PT    | 75.29        |
| Shift + Sign Flip | $S^3$ -Shift | 3        | R     | 75.75        |
|                   | <b>Ours</b>  | <b>2</b> | LVR   | <b>75.69</b> |
|                   | <b>Ours</b>  | <b>3</b> | LVR   | <b>76.36</b> |
|                   | <b>Ours</b>  | <b>4</b> | LVR   | <b>76.53</b> |
| ResNet-101        |              |          |       |              |
| Kernel            | Methods      | W Bits   | Init. | Top-1 (%)    |
| Multi.            | FP32         | 32       | R     | 77.37        |
| Shift + Sign Flip | <b>Ours</b>  | <b>2</b> | LVR   | <b>77.45</b> |
|                   | <b>Ours</b>  | <b>3</b> | LVR   | <b>77.93</b> |
|                   | <b>Ours</b>  | <b>4</b> | LVR   | <b>77.96</b> |

Table 2: Comparison of SOTA methods using DenseShift ResNet-50/101 architecture trained on ImageNet.

| Methods | Quantized Back | Extra | LVR Init | W Bits | mAP   |
|---------|----------------|-------|----------|--------|-------|
| FP32    | —              | —     | —        | 32     | 26.00 |
|         | ✓              | —     | —        | 3      | 26.23 |
| Ours    | ✓              | ✓     | ✓        | 3      | 25.75 |
|         | ✓              | ✓     | —        | 3      | 24.21 |

Table 3: DenseShift SSD300 v1.1 with ResNet-50 backbone finetuned on COCO object detection task.

2018; Qin et al. 2020), ternary weights (Li, Zhang, and Liu 2016; Shayer, Levi, and Fetaya 2017; Dong et al. 2017), PoT weights (Zhou et al. 2017; Elhoushi et al. 2019; Li et al. 2021) and more complex kernel (Zhang et al. 2018). We observe that DenseShift achieves SOTA performance on multiple network architectures and significantly outperforms the baseline with higher computational complexity.

### Transfer Learning

**Model and Dataset:** We use TorchVision implementation to verify the effectiveness and robustness of our proposed algorithm on transfer learning tasks. For object detection, we benchmark our proposed method on the bounding box detection track of MS COCO (Lin et al. 2014). As proof of concept, we use SSD300 v1.1 (Liu et al. 2016) with the obsolete VGG backbone replaced with ResNet-50 backbone. To demonstrate competitive performance, we use FCOS (Tian et al. 2019) with ResNet-50 backbone. For semantic segmentation, we benchmark our proposed method on a subset of MS COCO containing the 20 categories of Pascal VOC (Everingham et al. 2015). We use DeepLab V3 (Chen et al. 2017) with ResNet-50 backbone architecture. The DenseShift ResNet-50 backbone is trained from the previous section and we compare against full-precision baselines.

**Experiment Results:** Tables 3 and 4 illustrate that our 3-

| Methods | Quantized |     |      | W Bits | mAP  |
|---------|-----------|-----|------|--------|------|
|         | Back      | FPN | Head |        |      |
| FP32    | —         | —   | —    | 32     | 39.0 |
|         | ✓         | —   | —    |        | 39.3 |
|         | ✓         | ✓   | —    | 2      | 38.7 |
|         | ✓         | ✓   | ✓    |        | 37.1 |
|         | ✓         | —   | —    |        | 39.6 |
| Ours    | ✓         | ✓   | —    | 3      | 39.3 |
|         | ✓         | ✓   | ✓    |        | 37.7 |
|         | ✓         | —   | —    |        | 39.8 |
|         | ✓         | ✓   | —    | 4      | 39.6 |
|         | ✓         | ✓   | ✓    |        | 38.1 |

Table 4: DenseShift FCOS with ResNet-50 backbone finetuned on COCO object detection task.

bit SSD300 and FCOS achieve similar performance to their full-precision counterparts. Table 5 illustrate that our 3-bit DeepLab surpasses its full-precision counterpart. Without using our low-variance random initialization, the FCOS experiments using quantized feature-pyramid networks are unstable and failed to converge during training.

| Methods | Quantized |     |        | W Bits | mIoU | Global<br>Correct |
|---------|-----------|-----|--------|--------|------|-------------------|
|         | Back      | FPN | W Bits |        |      |                   |
| FP32    | —         | —   | 32     | 66.4   | 92.4 |                   |
|         | ✓         | —   |        | 65.8   | 92.2 |                   |
|         | ✓         | ✓   | 2      | 66.1   | 92.4 |                   |
| Ours    | ✓         | —   | 3      | 68.0   | 92.6 |                   |
|         | ✓         | ✓   |        | 67.4   | 92.8 |                   |
|         | ✓         | —   | 4      | 66.0   | 92.3 |                   |
|         | ✓         | ✓   |        | 66.3   | 92.0 |                   |

Table 5: DenseShift DeepLab V3 with ResNet-50 backbone finetuned on COCO semantic segmentation task.

## Speech Task

**Model and Datasets:** To further demonstrate the generalization of DenseShift networks, we experiment on an end-to-end spoken language (E2E SLU) task with ResNet-18 architecture. We benchmark our method on the Fluent Speech Commands (FSC) dataset. The FSC dataset (Lugosch et al. 2019a) comprised single-channel audio clips collected using crowd sourcing. Participants were requested to speak random phrases for each intent twice. The dataset contained 30,043 utterances spoken by 97 different speakers, each utterance contains three slots: action, object, and location. We considered a single intent as the combination of all the slots (action, object and location), resulting 31 intents in total.

**Experiment Results:** Results in table 6 are benchmarked against full-precision and SOTA shift networks performance. Our results demonstrates that our method can be applied to a field unrelated to the original CV field and can surpass full-precision performance as well.

| Method                 | W Bits | Val   | Test  |
|------------------------|--------|-------|-------|
| (Lugosch et al. 2019b) | 32     | 89.50 | 98.80 |
| (Avila et al. 2022)    | 2      | 90.66 | 98.41 |
|                        | 3      | 90.31 | 98.41 |
| <b>Ours</b>            | 2      | 90.73 | 98.60 |
|                        | 3      | 90.70 | 98.58 |

Table 6: DenseShift ResNet-18 architecture on End-to-End Spoken Language Understanding

## Conclusion

We present *DenseShift* with zero-free shifting and sign-scale decomposition for constructing high performance low-bit shift networks with high efficiency of training and inference. Such design eliminates the negative impact of weight freezing in existing low-bit power-of-two quantization mechanisms. We further improve the performance of DenseShift networks on transfer learning by introducing our low-variance random initialization strategy, which helps the networks to adapt to various tasks without severe performance degradation. Extensive experiments on a range of tasks demonstrate that DenseShift networks can outperform current SOTA shift networks in classification tasks, as well as obtains on-par performance with full-precision models in object detection and semantic segmentation tasks, which is a breakthrough for low-bit shift networks.

## References

Alizadeh, M.; Fernández-Marqués, J.; Lane, N. D.; and Gal, Y. 2018. An empirical study of binary neural networks’ optimisation. In *International Conference on Learning Representations*.

Avila, A. R.; Bibi, K.; Yang, R. H.; Li, X.; Xing, C.; and Chen, X. 2022. Low-bit Shift Network for End-to-End Spoken Language Understanding.

Bengio, Y. 2013. Estimating or Propagating Gradients Through Stochastic Neurons. *CoRR*, abs/1305.2982.

Cai, Z.; He, X.; Sun, J.; and Vasconcelos, N. 2017. Deep learning with low precision by half-wave gaussian quantization. In *Proceedings of the IEEE conference on computer vision and pattern recognition*, 5918–5926.

Chen, H.; Wang, Y.; Xu, C.; Shi, B.; Xu, C.; Tian, Q.; and Xu, C. 2020. AdderNet: Do we really need multiplications in deep learning? In *Proceedings of the IEEE/CVF Conference on Computer Vision and Pattern Recognition*, 1468–1477.

Chen, L.-C.; Papandreou, G.; Schroff, F.; and Adam, H. 2017. Rethinking Atrous Convolution for Semantic Image Segmentation. *arXiv:1706.05587*.

Courbariaux, M.; Bengio, Y.; and David, J.-P. 2015. Binaryconnect: Training deep neural networks with binary weights during propagations. In *Advances in neural information processing systems*, 3123–3131.

Deng, J.; Dong, W.; Socher, R.; Li, L.-J.; Li, K.; and Fei-Fei, L. 2009. Imagenet: A large-scale hierarchical image

database. In *2009 IEEE conference on computer vision and pattern recognition*, 248–255. Ieee.

Dong, Y.; Ni, R.; Li, J.; Chen, Y.; Zhu, J.; and Su, H. 2017. Learning accurate low-bit deep neural networks with stochastic quantization. *arXiv preprint arXiv:1708.01001*.

Elhoushi, M.; Chen, Z.; Shafiq, F.; Tian, Y. H.; and Li, J. Y. 2019. Deepshift: Towards multiplication-less neural networks. *arXiv preprint arXiv:1905.13298*.

Everingham, M.; Eslami, S. M. A.; Van Gool, L.; Williams, C. K. I.; Winn, J.; and Zisserman, A. 2015. The Pascal Visual Object Classes Challenge: A Retrospective. *International Journal of Computer Vision*, 111(1): 98–136.

Gudovskiy, D. A.; and Rigazio, L. 2017. Shiftcnn: Generalized low-precision architecture for inference of convolutional neural networks. *arXiv preprint arXiv:1706.02393*.

Han, S.; Mao, H.; and Dally, W. J. 2015. Deep compression: Compressing deep neural networks with pruning, trained quantization and huffman coding. *arXiv preprint arXiv:1510.00149*.

He, K.; Zhang, X.; Ren, S.; and Sun, J. 2015. Delving deep into rectifiers: Surpassing human-level performance on imagenet classification. In *Proceedings of the IEEE international conference on computer vision*, 1026–1034.

He, K.; Zhang, X.; Ren, S.; and Sun, J. 2016a. Deep residual learning for image recognition. In *Proceedings of the IEEE conference on computer vision and pattern recognition*, 770–778.

He, K.; Zhang, X.; Ren, S.; and Sun, J. 2016b. Identity mappings in deep residual networks. In *European conference on computer vision*, 630–645. Springer.

Hornik, K. 1991. Approximation capabilities of multilayer feedforward networks. *Neural networks*, 4(2): 251–257.

Hu, Q.; Wang, P.; and Cheng, J. 2018. From hashing to cnns: Training binary weight networks via hashing. In *Thirty-Second AAAI conference on artificial intelligence*.

Li, F.; Zhang, B.; and Liu, B. 2016. Ternary weight networks. *arXiv preprint arXiv:1605.04711*.

Li, X.; Liu, B.; Yu, Y.; Liu, W.; Xu, C.; and Partovi Nia, V. 2021. S3: Sign-Sparse-Shift Reparametrization for Effective Training of Low-bit Shift Networks. *Advances in Neural Information Processing Systems*, 34.

Li, Y.; Dong, X.; and Wang, W. 2019. Additive powers-of-two quantization: An efficient non-uniform discretization for neural networks. *arXiv preprint arXiv:1909.13144*.

Lin, T.-Y.; Maire, M.; Belongie, S.; Hays, J.; Perona, P.; Ramanan, D.; Dollár, P.; and Zitnick, C. L. 2014. Microsoft coco: Common objects in context. In *European conference on computer vision*, 740–755. Springer.

Lin, X.; Zhao, C.; and Pan, W. 2017. Towards Accurate Binary Convolutional Neural Network. *Advances in Neural Information Processing Systems*, 30.

Liu, W.; Anguelov, D.; Erhan, D.; Szegedy, C.; Reed, S.; Fu, C.-Y.; and Berg, A. C. 2016. Ssd: Single shot multibox detector. In *European conference on computer vision*, 21–37. Springer.

Liu, Z.; Wu, B.; Luo, W.; Yang, X.; Liu, W.; and Cheng, K.-T. 2018. Bi-real net: Enhancing the performance of 1-bit cnns with improved representational capability and advanced training algorithm. In *Proceedings of the European conference on computer vision (ECCV)*, 722–737.

Lugosch, L.; Ravanelli, M.; Ignoto, P.; Tomar, V. S.; and Bengio, Y. 2019a. Speech model pre-training for end-to-end spoken language understanding. *arXiv preprint arXiv:1904.03670*.

Lugosch, L.; Ravanelli, M.; Ignoto, P.; Tomar, V. S.; and Bengio, Y. 2019b. Speech Model Pre-training for End-to-End Spoken Language Understanding.

Miyashita, D.; Lee, E. H.; and Murmann, B. 2016. Convolutional Neural Networks using Logarithmic Data Representation. *arXiv:1603.01025*.

Prazeres, M. O.; Li, X.; Partovi Nia, V.; and Oberman, A. M. 2021. EuclidNets: Combining hardware and architecture design for Efficient Inference and Training.

Przewlocka-Rus, D.; Sarwar, S. S.; Sumbul, H. E.; Li, Y.; and De Salvo, B. 2022. Power-of-Two Quantization for Low Bitwidth and Hardware Compliant Neural Networks.

Qin, H.; Gong, R.; Liu, X.; Shen, M.; Wei, Z.; Yu, F.; and Song, J. 2020. Forward and backward information retention for accurate binary neural networks. In *Proceedings of the IEEE/CVF Conference on Computer Vision and Pattern Recognition*, 2250–2259.

Rastegari, M.; Ordonez, V.; Redmon, J.; and Farhadi, A. 2016. Xnor-net: Imagenet classification using binary convolutional neural networks. In *European conference on computer vision*, 525–542. Springer.

Shayer, O.; Levi, D.; and Fetaya, E. 2017. Learning discrete weights using the local reparameterization trick. *arXiv preprint arXiv:1710.07739*.

Tang, W.; Hua, G.; and Wang, L. 2017. How to train a compact binary neural network with high accuracy? In *Proceedings of the AAAI Conference on Artificial Intelligence*, volume 31.

Tian, Z.; Shen, C.; Chen, H.; and He, T. 2019. FCOS: Fully Convolutional One-Stage Object Detection.

Wang, Y.; Huang, M.; Han, K.; Chen, H.; Zhang, W.; Xu, C.; and Tao, D. 2021. AdderNet and its Minimalist Hardware Design for Energy-Efficient Artificial Intelligence. *arXiv preprint arXiv:2101.10015*.

Xu, Y.; Xu, C.; Chen, X.; Zhang, W.; Xu, C.; and Wang, Y. 2020. Kernel Based Progressive Distillation for Adder Neural Networks. In *NeurIPS*.

You, H.; Chen, X.; Zhang, Y.; Li, C.; Li, S.; Liu, Z.; Wang, Z.; and Lin, Y. 2020. ShiftAddNet: A Hardware-Inspired Deep Network. In *NeurIPS*.

Zhang, D.; Yang, J.; Ye, D.; and Hua, G. 2018. Lq-nets: Learned quantization for highly accurate and compact deep neural networks. In *Proceedings of the European conference on computer vision (ECCV)*, 365–382.

Zhou, A.; Yao, A.; Guo, Y.; Xu, L.; and Chen, Y. 2017. Incremental network quantization: Towards lossless cnns with low-precision weights. *arXiv preprint arXiv:1702.03044*.

Zhou, D.-X. 2020. Universality of deep convolutional neural networks. *Applied and computational harmonic analysis*, 48(2): 787–794.

## Proof of Theorems

**Theorem 1.** Every shift network has a DenseShift representation. More formally, suppose  $\hat{f}_{\mathbf{w}}(\mathbf{x}) = \sum_{j=1}^J \sum_{k=1}^{d_j} w_k h_k^j(\mathbf{x})$  is a shift network with output layer  $h^j(\mathbf{x}) = a(\mathbf{W}^j h^{j-1}(\mathbf{x}) + \mathbf{b}^j)$ , weights  $\mathbf{w} \in \{0\} \cup \{\pm 2^p\}$ , and activation function  $a(\cdot)$ , then there is a DenseShift network  $\hat{f}_{\mathbf{w}'}(\mathbf{x}) = \sum_{j=1}^J \sum_{k=1}^{d'_j} \mathbf{w}'_k h'_k(\mathbf{x})$ , with  $\mathbf{w}' \in \{\pm 2^p\}$  which equals  $\hat{f}_{\mathbf{w}}(\mathbf{x})$ .

*Proof.* The proof is straightforward by isolating zero shifts, and recreating these null weights in a larger DenseShift network with opposite weight signs. Define the  $j^{\text{th}}$  layer as

$$h^j(\mathbf{x}) = a(\mathbf{W}^j h^{j-1}(\mathbf{x}) + \mathbf{b}^j),$$

where  $h^0(\mathbf{x}) = \mathbf{x}$ ,  $J$  is the total number of layers each of output dimension  $d_j$  and  $\mathbf{W}$  of size  $d_j \times d_{j-1}$  can be a Toeplitz matrix for a convolutional layer,  $a(\cdot)$  is the activation function, and  $\mathbf{b}$  is the bias term. Define the shift network approximation of  $f(\mathbf{x})$  as

$$\hat{f}_{\mathbf{w}}(\mathbf{x}) = \sum_{j=1}^J \sum_{k=1}^{d_j} w_k h_k^j(\mathbf{x})$$

in which  $w_k \in \{0\} \cup \{\pm 2^p\}$  defines a shift network. We re-create an equivalent DenseShift network by isolating null weights  $w_k = 0$  and replacing them with a larger dense shift network of an arbitrary weights but with opposite signs. Now suppose  $\mathbf{w}_0 = \{k \mid w_k = 0\}$  and  $\mathbf{w}_1 = \{k \mid w_k \neq 0\}$  where  $\mathbf{w} = [\mathbf{w}_0^\top \mathbf{w}_1^\top]$ ,  $d_j = d_{0j} + d_{1j}$

$$\hat{f}_{\mathbf{w}}(\mathbf{x}) = \sum_{j=1}^J \left[ \sum_{k=1}^{d_{0j}} w_{0k} h_{0k}^j(\mathbf{x}) + \sum_{k=1}^{d_{1j}} w_{1k} h_{1k}^j(\mathbf{x}) \right].$$

Assume  $\tilde{\mathbf{w}} \in \{\pm 2^p\}$  is a nonzero shift arbitrary vector of elements  $\tilde{w}_{0k}$ ,

$$\begin{aligned} & \sum_{j=1}^J \left[ \sum_{k=1}^{d_{0j}} \mathbf{w}_{0k} h_{0k}^j(\mathbf{x}) + \sum_{k=1}^{d_{1j}} \mathbf{w}_{1k} h_{1k}^j(\mathbf{x}) \right] \\ &= \sum_{j=1}^J \left[ \sum_{k=1}^{d_{0j}} \tilde{\mathbf{w}}_k h_{0k}^j(\mathbf{x}) - \tilde{\mathbf{w}}_k h_{0k}^j(\mathbf{x}) + \sum_{k=1}^{d_{1j}} \mathbf{w}_{1k} h_{1k}^j(\mathbf{x}) \right] \end{aligned}$$

By defining  $\mathbf{w}' = [\tilde{\mathbf{w}}, -\tilde{\mathbf{w}}, \mathbf{w}_0]$  of increased size  $d'_j = d_{0j} + d_{1j} \geq d_j$ , one may rearrange terms and rewrite the neural approximate as

$$\hat{f}_{\mathbf{w}'}(\mathbf{x}) = \sum_{j=1}^J \sum_{k=1}^{d'_j} \mathbf{w}'_k h'_k(\mathbf{x}),$$

where  $h'_k$  is either  $h_{0k}^j$  or  $h_{1k}^j$  depending on the DenseShift weight  $\mathbf{w}'_k \in \{\pm 2^p\}$ .  $\square$

**Theorem 2.** DenseShift network with a  $L$ -Lischitz activation function is a universal approximator on a compact set  $K$  for any measurable continuous function  $f \in C(K)$  with

respect to the measure  $\mu$ , if the dense shift with weight and feature  $\mathbf{w}', \mathbf{x}'$  remains close to the regular network with weight and features  $\mathbf{w}, \mathbf{x}$  in the following sense

$$\int_K \left( \sum_{j=1}^J \sum_{k=1}^{d_j} (\mathbf{w}_k \mathbf{x}_k^j - \mathbf{w}'_k \mathbf{x}'_k^j) \right)^2 d\mu < \frac{\epsilon}{4L}$$

where  $\frac{\epsilon}{4}$  is the approximation quality of the regular neural network.

*Proof.* It is well-known that shallow networks are universal approximator (Hornik 1991) as well as deep networks (Zhou 2020). These results holds in infinity norm, so is also valid in  $\ell_p$  norm with  $p < \infty$ . For the simplicity of the mathematical mechanics here we only focus on the multilayer perceptron (Hornik 1991) on  $\ell_2$  norm

$$\|f - \hat{f}\| = \int_K |f(\mathbf{x}) - \hat{f}(\mathbf{x})|^2 d\mu \quad (7)$$

Suppose  $\hat{f}_{\mathbf{w}}$  is a real weight neural network and  $\hat{f}_{\mathbf{w}'}$  is a dense shift version of the same network  $\hat{f}_{\mathbf{w}}$ , of course with weights  $\mathbf{w}' \in \{\pm 2^p\}$ .

$$\|f - \hat{f}_{\mathbf{w}'}\| \quad (8)$$

$$= \int_K |f(\mathbf{x}) - \hat{f}_{\mathbf{w}'}(\mathbf{x}) \pm \hat{f}_{\mathbf{w}}(\mathbf{x})|^2 d\mu$$

$$= \int_K |f(\mathbf{x}) - \hat{f}_{\mathbf{w}}(\mathbf{x})|^2 d\mu \quad (9)$$

$$+ \int_K |\hat{f}_{\mathbf{w}}(\mathbf{x}) - \hat{f}_{\mathbf{w}'}(\mathbf{x})|^2 d\mu \quad (10)$$

$$+ 2 \int_K |[f(\mathbf{x}) - \hat{f}_{\mathbf{w}}(\mathbf{x})][\hat{f}_{\mathbf{w}}(\mathbf{x}) - \hat{f}_{\mathbf{w}'}(\mathbf{x})]| d\mu. \quad (11)$$

In order to show that shift networks are universal approximator it is enough to show that  $\|f - \hat{f}_{\mathbf{w}'}\|$  is bounded by an arbitrarily small  $\epsilon > 0$ . The first two terms (9)(10) are bounded by  $\frac{\epsilon}{4}$  (Hornik 1991), the second term is bounded by  $\frac{\epsilon}{4}$  given the shift net closeness assumption

$$\begin{aligned} & \int_K |\hat{f}_{\mathbf{w}}(\mathbf{x}) - \hat{f}_{\mathbf{w}'}(\mathbf{x})|^2 d\mu \\ &= \int_K \left( \sum_{j=1}^J \sum_{k=1}^{d_j} (\mathbf{w}_k \mathbf{x}_k^j - \mathbf{w}'_k \mathbf{x}'_k^j) \right)^2 d\mu \\ &\leq \int_K \left( \sum_{j=1}^J \sum_{k=1}^{d_j} (L \mathbf{w}_k \mathbf{x}_k^j - L \mathbf{w}'_k \mathbf{x}'_k^j) \right)^2 d\mu \\ &\leq \int_K \left( L \sum_{j=1}^J \sum_{k=1}^{d_j} (\mathbf{w}_k \mathbf{x}_k^j - \mathbf{w}'_k \mathbf{x}'_k^j) \right)^2 d\mu < \frac{\epsilon}{4}, \end{aligned}$$

Note that for the ReLU activation  $L = 1$ . The last term (11) is bounded by  $\frac{\epsilon}{2}$  the Cauchy-Schwartz inequality. So (7) is bounded by  $\epsilon$  by merging the pieces together.  $\square$

## Experiment Training Settings

### ImageNet Classification

**Model and Dataset:** We benchmark our proposed method with different bit-widths. To verify the effectiveness and robustness, we apply DenseShift to ResNet-18/50/101 architectures and evaluate on ILSVRC2012 dataset (Deng et al. 2009) with data augmentation and pre-processing strategy proposed in (He et al. 2016a). Following (Rastegari et al. 2016; Liu et al. 2018; Zhang et al. 2018), all but the first convolution layers are quantized.

**Training settings.** Following (Li et al. 2021), we train ResNet-18/50/101 backbones for 200 epochs using the cosine learning rate scheduler, with initial learning rate value of 1e-3. We use SGD as our optimizer, with a momentum and weight decay equal to 0.9 and 1e-4 respectively.

**Experiment Results:** Results are shown in table 1. We compare our proposed method with SOTA low-bit multiplication-free networks using binary weights (Rastegari et al. 2016; Cai et al. 2017; Hu, Wang, and Cheng 2018; Qin et al. 2020), ternary weights (Li, Zhang, and Liu 2016; Shayer, Levi, and Fetaya 2017; Dong et al. 2017), PoT weights (Zhou et al. 2017; Elhoushi et al. 2019; Li et al. 2021) and more complex kernel (Zhang et al. 2018). We observe that DenseShift achieves SOTA performance on multiple network architectures and significantly outperforms the baseline with higher computational complexity.

### Transfer Learning

**Model and Dataset:** We use TorchVision implementation to verify the effectiveness and robustness of our proposed algorithm on transfer learning tasks. For object detection, we benchmark our proposed method on the bounding box detection track of MS COCO (Lin et al. 2014). As proof of concept, we use SSD300 v1.1 (Liu et al. 2016) with the obsolete VGG backbone replaced with ResNet-50 backbone. To demonstrate competitive performance, we use FCOS (Tian et al. 2019) with ResNet-50 backbone. For semantic segmentation, we benchmark our proposed method on a subset of MS COCO containing the 20 categories of Pascal VOC (Everingham et al. 2015). We use DeepLab V3 (Chen et al. 2017) with ResNet-50 backbone architecture. The DenseShift ResNet-50 backbone is trained from the previous section and we compare against full-precision baselines.

**Training Settings:** Transfer learning tasks complete training process consist of two stages. In the first training stage, a backbone model obtains by pre-training the ImageNet classification task. In the second stage, the backbone and the extra layers of the train on the COCO dataset end-to-end. Our DenseShift SSD300 network is trained for a total of 130 epochs with a cosine learning rate scheduler. The initial learning rate is set to 2.6e-3. The network is optimized with an SGD optimizer. The momentum and weight decay are set to 0.9 and 5e-4 respectively. A linear warmup for the learning rate is used during the first training epoch only. Our DenseShift FCOS and DeepLab V3 networks follows the same training setup as their full-precision counterpart. We train our FCOS network for a total of 26 epochs with a multistep learning rate scheduler with milestones 16 and

22, gamma 0.1 and step size of 8. The initial learning rate is 0.01. The network is optimized with SGD optimizer with a weight decay value of 1e-4 and momentum value of 0.9. Automatic Mixed Precision (AMP) is used. We train our DeepLab V3 network for a total of 30 epochs with a lambda scheduler. The initial learning rate is set to 0.02. The network is optimized with an SGD optimizer with weight decay value of 1e-4 and momentum value of 0.9. The model is trained with a batch size of 4 and with auxiliary loss.

### Speech Tasks

**Model and Datasets:** To further demonstrate the generalization of DenseShift networks, we experiment on an end-to-end spoken language (E2E SLU) task with ResNet-18 architecture. We benchmark our method on the Fluent Speech Commands (FSC) dataset. The FSC dataset (Lugosch et al. 2019a) comprised single-channel audio clips collected using crowd sourcing. Participants were requested to speak random phrases for each intent twice. The dataset contained 30,043 utterances spoken by 97 different speakers, each utterance contains three slots: action, object, and location. We considered a single intent as the combination of all the slots (action, object and location), resulting 31 intents in total.

**Training Settings:** The network is trained on mini-batches of 8 samples for a total of 200 epochs following (Li et al. 2021). The initial learning rate is set to 0.0001 with a cosine learning rate scheduler. The SGD optimizer is used.

### Ablation Study

As mentioned in previous works (Alizadeh et al. 2018; Courbariaux, Bengio, and David 2015; Tang, Hua, and Wang 2017; Li et al. 2021), extra epochs are required for binary variables’ training due to their frequent sign variation instability. We verify the effects of both our LVR initialization strategy and increasing training epochs on the ImageNet classification task and summarize the results in Table 7. This demonstrates that low-variance random initialization has an insignificant impact when training from scratch.

| Network   | W Bits | LVR<br>Init | Epochs       |              |              |
|-----------|--------|-------------|--------------|--------------|--------------|
|           |        |             | 90           | 150          | 200          |
| ResNet-18 | 3      | —           | 69.27        | <b>70.03</b> | 70.33        |
|           |        | ✓           | <b>69.30</b> | 69.91        | <b>70.57</b> |

Table 7: Ablation study of low-variance random initialization and training epochs using 3-bit *DenseShift* ResNet-18 on ImageNet classification Top-1 accuracy.